The influence of non-thermal collisions in Europa's atmosphere

Shane R. Carberry Mogan[1], Andrew. R. Poppe[1], and Lucas Liuzzo[1]

[1]Space Sciences Laboratory, University of California, Berkeley, Berkeley, USA

Abstract

In this study, we show that non-thermal collisions can play a significant role in shaping Europa's exospheric structure. Collisions between radiolytically produced O_2 and the O produced via electron impact dissociation of O_2 play a significant role in affecting the exospheric structure and escape rates. Specifically, O+O_2 collisions lead to the production of a non-thermal O_2 population, and increase the O_2 escape while decreasing the O escape. These collisions are dependent on three specific physical parameters: (1) the density of O_2, (2) the electron impact dissociation rate of O_2, and (3) the O+O_2 collision cross section. We demonstrate here that O+O_2 collisions affect Europa's atmosphere even in the lowest limits considered. Thus, to more accurately determine the influence O+O_2 collisions have on Europa's atmosphere in preparation for the forthcoming spacecraft missions, Europa Clipper and the JUpiter ICy moons Explorer (JUICE), these physical parameters need to be better constrained.

Plain Language Summary

This study investigates the effects of collisions in Europa's atmosphere, specifically focusing on those involving oxygen atoms (O) and molecules (O_2). We find that collisions between O_2 produced within Europa's icy surface and the O it produces via dissociative processes while aloft in the atmosphere can affect the structure of Europa's atmosphere as well as the rates at which neutral particles escape to the local space environment. The study highlights three important factors that influence these collisions: the density of O_2 near Europa's surface, how often O_2 molecules are broken apart by electrons producing O, and the size of the O+O_2 collision cross section. Constraining these values is crucial for accurately modeling Europa's atmosphere in preparation for the forthcoming spacecraft missions, Europa Clipper and the JUpiter ICy moons Explorer (JUICE).

1 Introduction

As the icy Galilean satellites of Jupiter—Europa, Ganymede, and Callisto—are continuously overtaken and bombarded by the charged particles within the Jovian magnetosphere, the spatially and temporally varying precipitation of the incident magnetospheric plasma onto their icy surfaces and atmospheres lead to a myriad of complex processes. Neutral atoms (H, O) and molecules (H_2O, H_2, OH) are directly sputtered from these icy surfaces, while other molecules (O_2, H_2) are produced via radiolysis in the ice from which they subsequently release (e.g., Johnson 1990). The predominant radiolytic products in these atmospheres are molecular hydrogen and oxygen, where the former is primarily produced in a 2:1 stoichiometric ratio with the latter. Upon releasing from these icy surfaces, both molecular species accumulate in the atmospheres due to the infrequency of reactions occurring therein as well as the relatively low escape rates therefrom. Although O_2 and H_2 are expected to be the predominant species in these atmospheres near and far from the surfaces (e.g., Smyth and Marconi 2006, Marconi 2007, Carberry Mogan et al. 2022), respectively, only emissions from their dissociated products H and O have actually been detected in the gas-phase (e.g., Hall et al. 1995, 1998, Cunningham et al. 2015, Roth et al. 2016, 2017a,b, Roth 2021, Roth et al. 2021). Although these atoms can be produced directly via sputtering of ice (e.g., Bar-Nun et al. (1985), Kimmel and Orlando (1995)), they are primarily produced via dissociative processes of their parent molecules in the atmosphere (e.g., Vorburger et al. 2024).

Numerical models have been extensively applied to the icy Galilean satellites' atmospheres over the years to characterize and predict key aspects therein. At Callisto, it has been established that collisions must be considered in its atmosphere, e.g., via molecular kinetics (MK) models (Carberry Mogan et al., 2020, 2021b,a, 2022). At Ganymede, there is not yet a consensus on whether models of its atmosphere should include collisions (e.g., Marconi 2007, Leblanc et al. 2017, Waite Jr et al. 2024) or neglect them (e.g., Turc et al. 2014, Leblanc et al. 2023, Vorburger et al. 2022, 2024). However, if a study were carried out focusing on the influence of non-thermal collisions in Ganymede's atmosphere, such as that for H_2+H collisions in Callisto's atmosphere (Carberry Mogan et al., 2022) or the work presented here for O_2+O collisions in Europa's atmosphere, a similar conclusion is likely: they should be considered.

At Europa, the topic of this study, collisions were considered in models of the atmosphere pre-2006 (Saur et al., 1998, Shematovich and Johnson, 2001, Shematovich et al., 2005, Shematovich, 2006, Smyth and Marconi, 2006), but more recent models have since neglected them (Cassidy et al., 2007, Plainaki et al., 2010, 2012, 2013, Teolis et al., 2017, Vorburger and Wurz, 2018, Oza et al., 2019). Including collisions would not significantly affect the results presented in some of these studies (Cassidy et al., 2007, Oza et al., 2019) which focused on reproducing observed atmospheric asymmetries (McGrath et al., 2004, Roth et al., 2016) as a result of surface interactions. However, collisionless models in other studies were implemented under the assumption that if the atmosphere is too thin for O_2 molecules to frequently collide with one another, then collisions between *all* species can be neglected when modeling Europa's atmosphere (Plainaki et al., 2010, 2012, 2013, Vorburger and Wurz, 2018), which other models have since used for their own justification (Lucchetti et al., 2016, Teolis et al., 2017). Here we demonstrate that, under closer scrutiny, this assumption does not hold. Indeed, if the same calculations used to justify a collisionless model according to

Europa's O_2 component were applied to other atmospheric species, such as the O produced via electron impact dissociation of O_2, they would indicate that collisions occur (see Suppl. Mat.).

We simulate collisions in Europa's atmosphere using a MK model with inputs for its O_2, H_2, O, and H components consistent with values suggested in the literature. As will be seen, it is the *non-thermal* collisions, particularly those between radiolytically produced O_2 and the hot O ($\sim$eV) primarily produced via electron impact dissociation of O_2, that have a significant effect on escape rates and the structure of Europa's atmosphere. Although the extent to which these collisions affect atmospheric escape and structure varies as a function of modeling inputs (e.g., surface densities, collision cross sections, and electron impact reaction rates), we demonstrate here that these collisions are non-negligible even in the lowest limits of the parameter space explored (i.e., the smallest collision cross section and lowest surface densities and electron impact reaction rates considered). Thus, collisions should be taken into account when modeling Europa's atmosphere.

Note that we are not attempting to provide a comprehensive model of Europa's atmosphere. Instead, our aim is to isolate the influence non-thermal collisions can have in Europa's atmosphere, and thus neglect other non-thermal sources, such as sputtering and interactions with the ionosphere (e.g., Dols et al. 2016). Future work will look to provide a more comprehensive model by including (and comparing) the influences of these processes.

2 Method

2.1 Molecular Kinetics Model

To simulate Europa's atmosphere and the influence of collisions therein we implement the direct simulation Monte Carlo (DSMC) method (Bird, 1994). The DSMC method is a molecular kinetics model which simulates macroscopic gas dynamics via stochastic microscopic processes using computational particles, each representing many real atoms (O and H) or molecules (O_2 and H_2). The model implemented here was initially developed to simulate Callisto's tenuous atmosphere (Carberry Mogan et al., 2020, 2021b,a, 2022), and has been adapted here to simulate Europa's atmosphere.

A 1D spherically symmetric simulation domain is employed in which radial cells span from Europa's surface, $r_0 = R_E = 1560.8$ km, to its Hill sphere, $r_{\rm HS} \sim 8.7 R_E$. If a particle's trajectory crosses either of these boundaries, they are removed from the simulation and loss rates are calculated accordingly (see Suppl. Mat.). This network of cells allows for particles to be locally grouped based on their position to simulate collisions as well as to take samples and calculate averages of the macroscopic flow. For further details on this DSMC model, we refer the reader to our earlier publications (e.g., Carberry Mogan et al. 2022) and the Supplemental Material. We note that although our 1D model is inherently incapable of capturing local asymmetries in Europa's atmosphere (e.g., Oza et al. 2019), but neglecting such features do not affect the principal conclusions of this study.

2.2 Model Uncertainties

2.2.1 Surface Densities of O_2 and H_2

For O_2 and H_2, we implement steady-state thermal outgassing fluxes (see Suppl. Mat.) calculated as a function of a prescribed surface density, n_0, which we vary over three orders of magnitude: $n_{0,O_2} = 10^7$ cm^{-3}, 10^8 cm^{-3}, and 10^9 cm^{-3}; $n_{0,H_2} = 10^5$ cm^{-3}, 10^6 cm^{-3}, and 10^7 cm^{-3}. These values for n_{0,O_2} (and the corresponding column densities) fall within the broad range of those suggested in the literature (e.g., Johnson et al. 1982, Eviatar et al. 1985, Hall et al. 1995, Kliore et al. 1997, Saur et al. 1998, Hall et al. 1998, Ip et al. 1998, Johnson et al. 1998, Hansen et al. 2005, Shematovich and Johnson 2001, Shematovich et al. 2005, Shematovich 2006, Saur et al. 2011, Plainaki et al. 2012, Roth et al. 2016, Teolis et al. 2017, Vorburger and Wurz 2018). Similarly, $n_{0,H_2} = 10^5$ cm^{-3} and 10^6 cm^{-3} fall within the much more limited range of those suggested in the literature (e.g., Smyth and Marconi 2006, Szalay et al. 2024), with $n_{0,H_2} = 10^7$ cm^{-3} presenting an upper-bound case.

2.2.2 Electron Impact Reaction Rates

While aloft in the atmosphere, these molecules are susceptible to electron impacts, resulting in dissociation and/or ionization (see Suppl. Mat.). If nascent H or O atoms are produced via electron impact dissociation, representative particles are injected into the simulation domain and subsequently tracked. The range of frequencies (hereafter referred to as rates) for electron impact reactions implemented in this study are taken from a recent study which analyzed the local electron environment in Europa's orbit and wake during Juno flybys (Szalay et al., 2024) (see Suppl. Mat.). Szalay et al. (2024) demonstrated that these reaction rates can vary significantly, in some instances over an order of magnitude (see Extended Table 3 in Szalay et al. 2024).

2.2.3 Collision Cross Sections

Often in molecular kinetics simulations the biggest uncertainties stem from the implemented collision cross sections, σ. Elastic collisions between O_2 and H_2 particles are simulated using the variable hard sphere model (Bird, 1994). Elastic collisions between the non-thermal O and H atoms and the O_2 and H_2 molecules are simulated using the model derived by Lewkow and Kharchenko (2014), "LK14." Unfortunately for the purposes of this study, $O+O_2$ collisions have not been studied as in-depth as other atom-molecule collisions, such as $O+N_2$ (Balakrishnan et al., 1998, Kumar et al., 2023), at the energies relevant to this study. Instead, this collision has been studied at energies far larger (0.5–5.0 keV) than those relevant to Europa's atmosphere (Schafer et al., 1987). In addition, since O and O_2 have low-lying electronic states, collisions between excited oxygen atoms and molecules have been studied in more detail (e.g., Miura et al. 2002, Pan et al. 2019).

The LK14 model used here to derive σ_{O+O_2} (red lines in Fig. 1) was originally developed to simulate keV protons precipitating into Mars' upper atmosphere. Although the model was utilized for a different energy regime than the work presented here ($\lesssim$eV), the authors suggested σ can be scaled according to the masses of the colliding species as well as the collision energy.

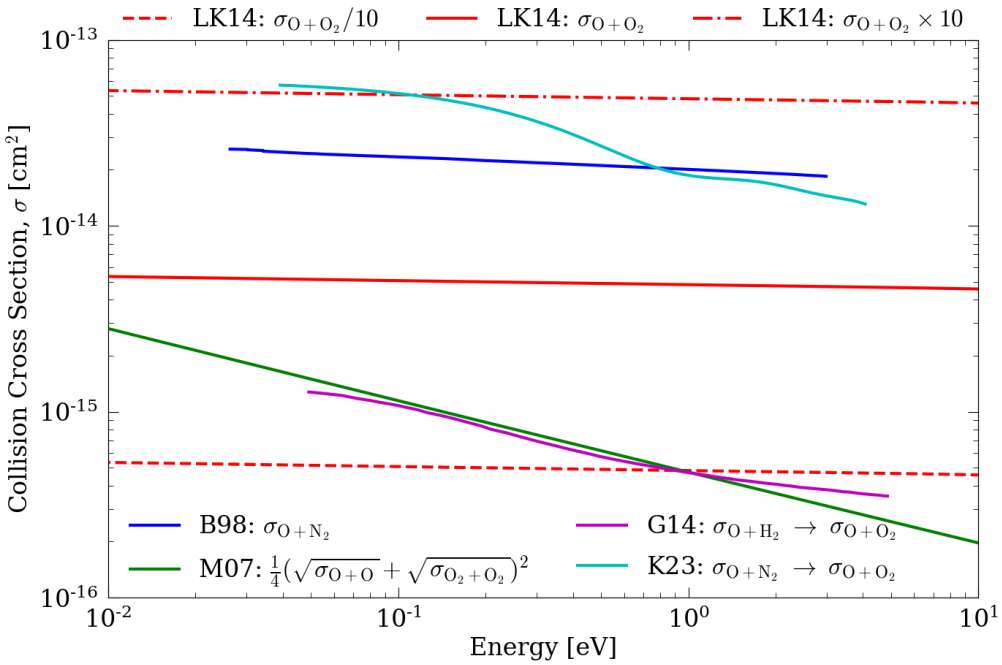

Figure 1: Collision cross sections, σ, implemented in this study for $O+O_2$ collisions (red lines) compared to similar σ derived in the literature. Balakrishnan et al. (1998), "B98" (blue), calculated σ_{O+N_2}; Marconi (2007), "M07" (green) calculated σ_{O+O_2} as an average of σ_{O+O} and $\sigma_{O_2+O_2}$;Gacesa and Kharchenko (2014), "G14" (magenta) calculated σ_{O+H_2}, which we mass-scaled to σ_{O+O_2}; and Kumar et al. (2023), "K23" (cyan), calculated σ_{O+N_2}, which we mass-scaled to σ_{O+O_2}.

In Fig. 1 we compare σ_{O+O_2} implemented here to σ calculated for O and other diatomic molecules, N_2 (Balakrishnan et al., 1998, Kumar et al., 2023) and H_2 (Gacesa and Kharchenko, 2014). A recent calculation for σ_{O+N_2} has been provided by Kumar et al. (2023), "K23," which we mass-scale to σ_{O+O_2} (see Suppl. Mat.). Below ∼0.1 eV, the mass-scaled σ_{O+N_2} is ∼10× larger than σ_{O+O_2} derived via the LK14 model, and the former approaches the latter with increasing energy to within a factor of ∼2 by ∼5 eV. We also mass-scaled σ_{O+H_2} calculated by Gacesa and Kharchenko (2014), "G14," to σ_{O+O_2}, which is seen to be at least ∼5× smaller than σ_{O+O_2} derived via the LK14 model throughout the considered energy range, and the discrepancy grows with increasing COM energy.

In an earlier DSMC model of Europa's atmosphere, Shematovich (2006) directly substituted σ_{O+N_2} calculated by Balakrishnan et al. (1998), "B98," for σ_{O+O_2}, which is ∼5× larger than σ_{O+O_2} derived via the LK14 model. While Smyth and Marconi (2006) did not explicitly list the value they used for σ_{O+O_2}, insight can be gained from a subsequent work by one of the authors involved. Marconi (2007), "M07," implemented a 2D DSMC model to simulate Ganymede's atmosphere composed of the same species as that of Europa, and σ_{O+O_2} was calculated as an average of σ_{O+O} and $\sigma_{O_2+O_2}$ derived elsewhere in the literature (see Table 3 and references therein). As can be seen, the resultant M07 distribution closely resembles the mass-scaled σ_{O+H_2}.

Thus, the σ_{O+O_2} we implement here lies somewhere in between that implemented in other

DSMC models and the σ of O with other diatomic molecules. Therefore, to determine the influence of σ_{O+O_2} on our simulation results, we increased (dash-dotted red line in Fig. 1) and decreased (dashed red line in Fig. 1) σ_{O+O_2} derived via the LK14 model by a factor of 10 to more closely resemble these other σ. It should also be noted that the LK14 model has been used to simulate the same non-thermal collisions as those considered here in more recent DSMC models of the water-product atmospheres on Ganymede (Leblanc et al., 2017) and Callisto (Carberry Mogan et al., 2022). Thus, it is not without merit to apply the LK14 model to simulate non-thermal collisions in Europa's atmosphere.

3 Results

3.1 Non-Thermal Density Profiles

Fig. 2 illustrates the density profiles for H_2, O_2, H, and O as a function of altitude for the prescribed surface densities, n_0, of O_2 (n_{0,O_2} = 10^7 cm^{-3}, 10^8 cm^{-3}, and 10^9 cm^{-3}) with n_{0,H_2} = 10^5 cm^{-3}. With increasing n_{0,O_2} the influence collisions have non-linearly increases compared to simulations which neglect such collisions. For example, with increasing n_{0,O_2} the production of hot O via electron impacts increases, but the initially hot O is more efficiently thermalized by collisions with a more dense O_2 component. As a result, the O density significantly increases relative to a simulation in which such collisions are neglected: with n_{0,O_2} = 10^7 cm^{-3}, there is a negligible difference in O density when collisions are considered versus when they are neglected; with n_{0,O_2} = 10^8 cm^{-3}, the O density effectively doubles within ~1000 km of the surface as a result of collisions with O_2; and with n_{0,O_2} = 10^9 cm^{-3}, the O density is enhanced by almost two orders of magnitude near the surface. As the hot O component thermalizes via O+O_2 collisions, the initially thermal O_2 component is heated; and a larger n_{0,O_2} results in more hot O being produced, which in turn inflates the non-thermal O_2 component due to more frequent O+O_2 collisions. Also with n_{0,O_2} = 10^9 cm^{-3}, the densities of the H_2 and H components are diminished over the same altitude range in which the O densities are enhanced. This is due to the H_2 having to diffuse through a much denser O_2 component, which can knock more H_2 particles back down to the surface, which is treated as a sink in our steady-state model, thereby inhibiting their otherwise upward trajectories and reducing atmospheric escape (illustrated later in Fig. 4). As a result, the density of the H produced by H_2 is also reduced.

3.2 Influence of Model Uncertainties

In Figure 3, we show results from case studies where we fixed n_{0,H_2} and n_{0,O_2} at their respective median values, 10^6 cm^{-3} and 10^8 cm^{-3}, and varied σ_{O+O_2} and electron impact dissociation rates. When collisions are neglected, the resultant density profile is isothermal, whereby the density effectively drops off as a function of the local scale height, $H \sim 25$ km, calculated according to the prescribed surface temperature, $T_0 = 125$ K. When collisions are included, however, the O_2 component is heated via O+O_2 collisions, resulting in a sharp transition in H. Depending on the implemented electron impact dissociation rate (0.56–5.6×10^{-6} s^{-1}) and σ_{O+O_2} (Fig. 1), the altitude at which this transition occurs varies from ~100 km to

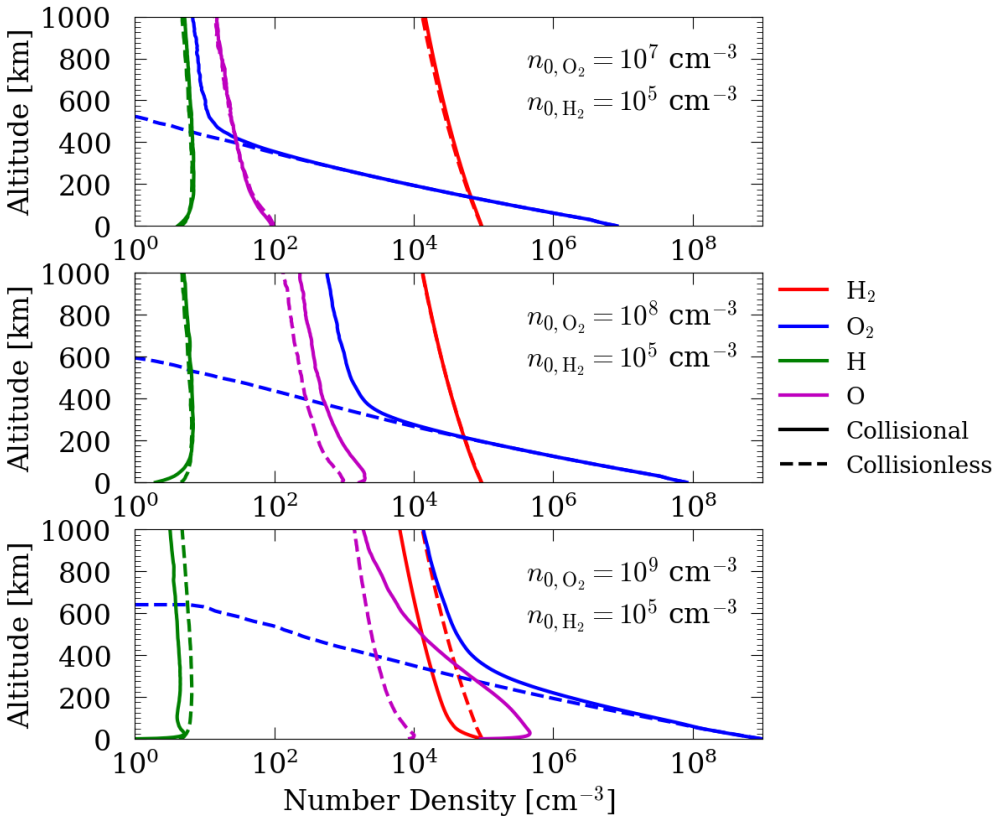

Figure 2: Density profiles for H_2 (red), O_2 (blue), H (green), and O (magenta) as a function of altitude for the prescribed surface densities, n_0, of O_2 (top: $n_{0,O_2} = 10^7$ cm^{-3}, middle: $n_{0,O_2} = 10^8$ cm^{-3}, and bottom: $n_{0,O_2} = 10^9$ cm^{-3}) with $n_{0,H_2} = 10^5$ cm^{-3} in DSMC simulations which included (solid lines) and neglected (dashed lines) collisions.

~400 km and the corresponding non-thermal O_2 density at an altitude of ~1000 km varies from ~10^4 cm^{-3} to ~10^2 cm^{-3}, respectively. When electron impact dissociation rates are kept the same but σ_{O+O_2} is reduced by a factor of 10, the altitude at which this transition occurs increases and, thus, the density of the non-thermal O_2 component decreases; i.e., with a smaller σ_{O+O_2}, fewer $O+O_2$ collisions occur such that the O_2 component is heated less. However, even when implementing these relatively small σ_{O+O_2}, $O+O_2$ collisions can still significantly affect the O_2 density profile.

Interestingly, the radial profile of the non-thermal O_2 component produced via $O+O_2$ collisions resembles that of O_2 sputtered from the surface with a high-energy tail in exospheric models of Europa's atmosphere (e.g., Plainaki et al. 2012, Teolis et al. 2017, Vorburger and Wurz 2018). Depending on the electron impact dissociation rate and σ_{O+O_2}, however, these collisions can produce more non-thermal O_2 than can sputtering. The non-thermal O_2 component produced via $O+O_2$ collisions is also consistent with earlier DSMC models of Europa's atmosphere (Shematovich, 2006, Smyth and Marconi, 2006) which also included such collisions. In the upper limit case considered here, when the electron impact dissociation rate is 5.6×10^{-6} s^{-1} and σ_{O+O_2} derived by the LK14 model is enhanced by a factor of 10, the non-thermal O_2 component produced is more dense than that of the models of Smyth

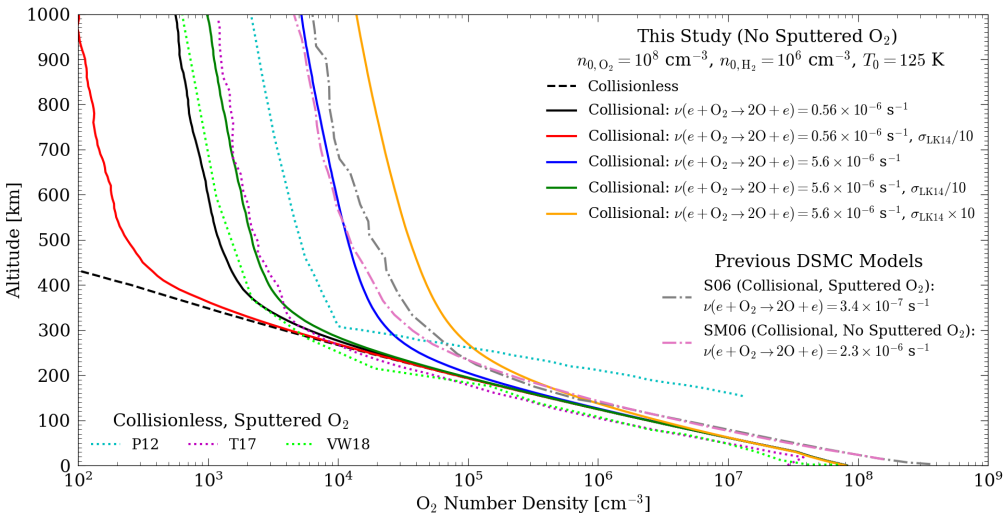

Figure 3: O_2 density profiles from DSMC simulations in which collisions were included (solid colored lines) and neglected (dashed black line), and the electron impact dissociation rate, ν, and O+O_2 collision cross section, σ_{O+O_2}, were varied. Results are also compared to those of earlier DSMC models of Europa's atmosphere (dash-dotted lines; Shematovich 2006, "S06," grey, and Smyth and Marconi 2006, "SM06," pink) as well as collisionless models which included sputtering as the lone non-thermal source of O_2 (dotted lines; Plainaki et al. 2012, "P12," cyan, Teolis et al. 2017, "T17," magenta, and Vorburger and Wurz 2018, "VW18," lime green).

and Marconi (2006) and Shematovich (2006) by ∼150 km despite their n_{0,O_2} being larger.

The differences in results from our DSMC model to those of Smyth and Marconi (2006) and Shematovich (2006) are due to the different modeling inputs. Smyth and Marconi (2006) implemented a different electron impact reaction rate (2.6×10^{-6} s^{-1}; c.f., Fig. 3), initial speed of hot O (1.85 km/s; c.f., Suppl. Mat.), and σ_{O+O_2} (see M07 in Fig. 1) compared to those considered here. Shematovich (2006) included the high-energy tail for sputtered O_2, a smaller electron impact dissociation rates (3.4×10^{-7} s^{-1}; c.f., Fig. 3), a different initial speed distribution of hot O produced via electron impacts (Cosby 1993; c.f., Suppl. Mat.), and a different σ_{O+O_2} (see B98 in Fig. 1). Note Shematovich (2006) also considered photodissociation of O_2 and dissociative recombination of O_2^+ as additional sources for hot O, but we only compare our results to their model in which electron impact dissociation of O_2 was the sole source. Shematovich (2006) assumed a relatively small electron impact reaction rate, so that their assumed photodissociation rate (1.8×10^{-7} s^{-1}; see Table 2 in Shematovich et al. 2005) produced a comparable amount of O. In contrast, we assumed electron impact dissociation rates ∼2–20× larger than Shematovich (2006)—and even larger rates are expected (Szalay et al., 2024). Shematovich (2006) also assumed a smaller excess energy for photodissociation than electron impact dissociation, so that the O produced via the former were more likely to thermalize via collisions with O_2 than the O produced via the latter. As a result, a ∼1 order of magnitude denser O component was produced when both of these sources were considered as opposed to only electron impact dissociation (see Fig. 5 in Shematovich et al. 2005). Including photodissociation of O_2 in our models would

have a negligible effect on our results. Furthermore, Shematovich (2006) also considered a case where dissociative recombination of O_2^+ was the sole source of O, but a negligible amount was produced compared to dissociation of neutral O_2. Thus, we can safely neglect this non-thermal source of O as well.

3.3 Atmospheric Escape

Fig. 4 illustrates the influence non-thermal collisions also have on neutral escape rates from Europa's atmosphere. Since we assume O_2 thermally desorbs from Europa's icy surface (see Suppl. Mat.) and neglect the high-energy tail of the velocity distribution for sputtered O_2, there is no O_2 escape when we neglect collisions. Thus, the only escape mechanism for O_2 considered here is due to collisions with hot H and O. Therefore, in the top panel of Fig. 4 we plot the simulated O_2 escape rates only from the simulations in which collisions are considered. Increasing the electron impact dissociation rate causes an increase in the O_2 escape rate, as the production of more non-thermal O leads to a greater number of O+O_2 collisions (as well as a more dense non-thermal O_2 component, Fig. 3).

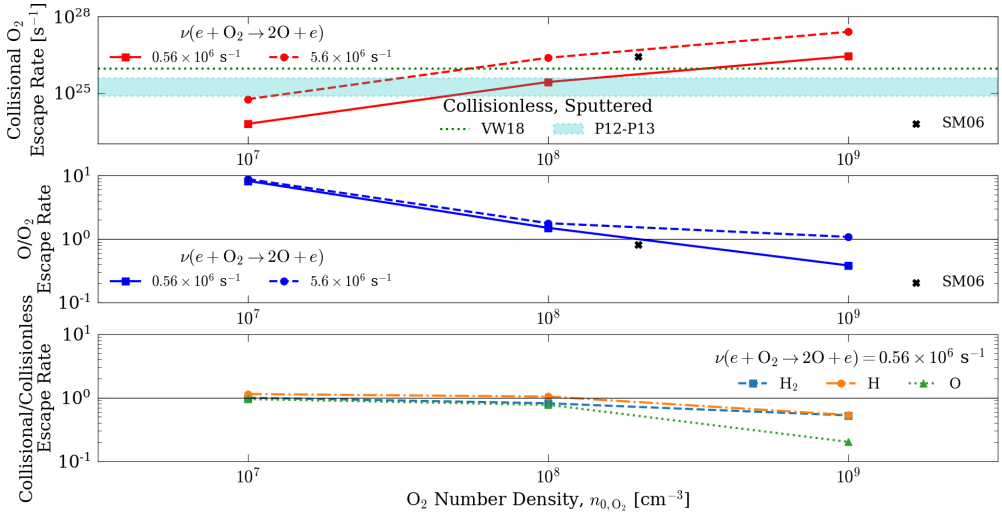

Figure 4: *Top*: O_2 escape rates induced via non-thermal collisions. Results are shown for a range of prescribed n_{O_2} (with n_{H_2} fixed to 10^6 cm^{-3}) as well as electron impact dissociation rates, ν, and are compared to those from Smyth and Marconi (2006), "SM06," Plainaki et al. (2012, 2013), "P12-13," and Vorburger and Wurz (2018), "VW18." *Middle*: Ratio of escape between O and O_2 as a function of n_{O_2} and ν and compared to that from SM06. *Bottom*: Ratio of escape rates between simulations with and without collisions for H_2 (dashed blue line), H (dash-dotted orange line), and O (dotted green line).

We compare the range of simulated O_2 escape rates to that of Smyth and Marconi (2006), who also only simulated thermally desorbing O_2 so that the only escaping O_2 was due to non-thermal collisions. Although Smyth and Marconi (2006) implemented different modeling inputs (see Section 3.2), their simulated O_2 escape rates align nicely with those of this study within the range of electron impact dissociation rates considered. We also compare our simulated escape rates to those from models of Europa's atmosphere where sputtering of

O_2 was considered but collisions were neglected (Plainaki et al., 2012, 2013, Vorburger and Wurz, 2018). That is, in these collisionless models O_2 only escapes as a result of the high-energy tail of its initial velocity distribution. As can be seen, depending on n_{0,O_2} and the electron impact dissociation rate, O+O_2 collisions can lead to significantly more O_2 escape than can sputtering.

In the simulations in which collisions are considered, we also examined the ratio of O escape to that of O_2 (middle panel of Fig. 4). With $n_{0,O_2} = 10^7$ cm^{-3}, the ratio of O-to-O_2 escape is ∼9 regardless of the electron impact dissociation rate. This is consistent with the O density profile with and without collisions shown in Fig. 2; i.e., with $n_{0,O_2} = 10^7$ cm^{-3}, O+O_2 collisions do not noticeably affect the O component. However, for $n_{0,O_2} \gtrsim 10^8$ cm^{-3}, a non-linear relationship between the simulated escape rates and these collisions is demonstrated as the O-to-O_2 escape ratios begin to significantly diverge from one another. When the electron impact dissociation rate is enhanced by a factor of 10, the O_2 escape is similarly enhanced (top panel in Fig. 4). However, the same is not true for the escaping hot O: with $n_{0,O_2} \gtrsim 10^9$ cm^{-3}, the ratio of O-to-O_2 escape with an electron impact dissociation rate of 5.6×10^{-6} s^{-1} is ∼3× more than that with a rate of 0.56×10^{-6} s^{-1} (O escapes 20× more in the former simulation than in the latter). Moreover, with $n_{0,O_2} \gtrsim 10^9$ cm^{-3} and an electron impact dissociation rate of 0.56×10^{-6} s^{-1}, more O_2 escapes than O. Smyth and Marconi (2006) predicts slightly less atomic O escape than in our models, which, again, is likely a result of the difference in modeling inputs mentioned above. However, both Smyth and Marconi (2006) and our simulations with an electron impact dissociation rate of 0.56×10^{-6} s^{-1} suggest that for $n_{0,O_2} \gtrsim 3\times10^8$ cm^{-3} more oxygen will escape Europa's atmosphere in molecular form rather than atomic.

Finally, in the bottom panel of Fig. 4 we compare the ratios of escape rates for the H_2, H, and O components from simulations in which collisions are considered compared to when they are neglected across the range of n_{0,O_2} considered with $n_{0,H_2} = 10^6$ cm^{-3}. For all three species, collisions with O_2 suppress escape compared to simulations without collisions, with O being the most affected; e.g., with $n_{0,O_2} = 10^9$ cm^{-3}, the O escape rate is reduced by ∼5. Since we simulate H_2 thermally desorbing from the surface, one can analytically calculate the expected escape rates in a collisionless simulation via the Jeans formula according to n_0 and T_0 (e.g., Carberry Mogan et al. 2020). As can be seen, however, collisions with a much denser O_2 component result in *sub*-Jeans escape, making analytically estimating thermal H_2 escape more difficult.

4 Conclusion

Here we have demonstrated that collisions can play a significant role in shaping Europa's exospheric structure. Non-thermal collisions between the O_2 component, the most dense species near the surface, and the hot O it produces via electron impact dissociation produces a significant non-thermal O_2 population and enhances O_2 escape. Comparing our simulation results to those of collisionless models in which sputtering is the lone non-thermal source of O_2 (Plainaki et al., 2012, 2013, Teolis et al., 2017, Vorburger and Wurz, 2018) suggests that larger non-thermal O_2 densities and escape rates can result from these collisions than from sputtering. This result complicates the idea often posited for surface bound exospheres

produced as a result of magnetospheric plasma bombardment (Plainaki et al., 2018, Szalay et al., 2024): that if an otherwise thermal component of the atmosphere (e.g., O_2) is detected at high altitudes, e.g., by an in-situ spacecraft, then it was likely sputtered in order to obtain the energy required to reach such heights; and knowing that this detected species comes directly from the surface, these observations can be used to extrapolate information about the surface, such as source rates and composition. However, we have demonstrated that non-thermal O_2 can reach these same altitudes as a result of $O+O_2$ collisions, and as such, inferring information about the surface becomes more complicated.

Since previous collisionless models did not account for sputtered O_2 molecules depositing their energy within a collisional atmosphere, their simulated neutral O_2 escape rates due to sputtering should be considered as *upper limits*. In addition, we show that as the O_2 density increases, the escape rates of H_2, H, and O decrease, again suggesting that the escape rates presented for these species by collisionless models should also be considered as upper limits. Thus, a model of Europa's atmosphere must take into account collisions *and* sputtering to determine the total atmospheric escape rates, from which surface composition and evolution can be inferred (e.g., Szalay et al. 2024) as well as the source rates for a neutral torus can be derived (e.g., Smith et al. 2019, Szalay et al. 2022).

Finally, the influence of non-thermal collisions in Europa's atmosphere are largely dependent on three key physical parameters: the surface density of O_2, the electron impact dissociation rates which produce hot O, and the collision cross sections implemented to simulate $O+O_2$ collisions. Whereas the first two parameters implemented here are taken from established values in the literature, the $O+O_2$ collision cross section was roughly approximated using a scaling model from the literature. Although we varied the size of this collision cross section to resemble those in the literature for similar collisions, future work can improve on this treatment by deriving this collision cross section, e.g., in a manner similar to recent studies which derived collision cross sections for hot O colliding with molecules present in other topical planetary atmospheres (e.g., Gacesa et al. 2020, Chhabra et al. 2023, Kumar et al. 2023). Indeed, this collision has been shown here to be crucial in affecting the evolution of Europa's atmosphere, and likely has a similar influence on the O_2-rich atmospheres of the other icy Galilean satellites, Ganymede and Callisto, all of which are soon to be the subject of upcoming spacecraft missions (Clipper and JUICE). Moreover, the influence of this collision will likely affect the interpretation of the Juno flyby of Europa from which O_2 production rates were inferred (Szalay et al., 2024): the pick-up ions detected by Juno suggested a highly non-thermal population in Europa's atmosphere; however, only atmospheric and direct surface sputtering and/or Joule heating were considered as a possible heating mechanism, and not non-thermal collisions like those presented here.

Acknowledgments

The authors acknowledge support from NASA Solar System Workings grants 80NSSC21K0152 and 80NSSC22K0097.

Open Research

Results used in this study can be found in Carberry Mogan et al. (2024).

References

Balakrishnan, N., Kharchenko, V., and Dalgarno, A. (1998). Slowing of energetic $O(^3P)$ atoms in collisions with N_2. *Journal of Geophysical Research: Space Physics*, 103(A10):23393–23398.

Bar-Nun, A., Herman, G., Rappaport, M. L., and Mekler, Y. (1985). Ejection of H_2O, O_2, H_2 and H from water ice by 0.5–6 keV H^+ and Ne^+ ion bombardment. *Surface science*, 150(1):143–156.

Bird, G. A. (1994). *Molecular gas dynamics and the direct simulation of gas flows*.

Brinkmann, R. T. (1970). Departures from Jeans' escape rate for H and He in the Earth's atmosphere. *Planetary and Space Science*.

Carberry Mogan, S. R., Liuzzo, L., and Poppe, A. R. (2024). Data for "The influence of non-thermal collisions in Europa's atmosphere" by Carberry Mogan et al. (2024). Available at https://doi.org/10.5281/zenodo.10892311.

Carberry Mogan, S. R., Tucker, O. J., and Johnson, R. E. (2021a). The influence of upper boundary conditions on molecular kinetic atmospheric escape simulations. *Planetary and Space Science*, 205:105302.

Carberry Mogan, S. R., Tucker, O. J., Johnson, R. E., Roth, L., Alday, J., Vorburger, V., Wurz, P., Galli, A., Smith, H. T., Marchand, B., and Oza, A. V. (2022). Callisto's atmosphere: First evidence for H_2 and constrains on H_2O. *Journal of Geophysical Research: Planets*.

Carberry Mogan, S. R., Tucker, O. J., Johnson, R. E., Sreenivasan, K. R., and Kumar, S. (2020). The influence of collisions and thermal escape in Callisto's atmosphere. *Icarus*.

Carberry Mogan, S. R., Tucker, O. J., Johnson, R. E., Vorburger, A., Galli, A., Marchand, B., Tafuni, A., Sahin, I., Sreenivasan, K. R., and Kumar, S. (2021b). A tenuous, collisional atmosphere on Callisto. *Icarus*.

Cassidy, T. A., Johnson, R. E., McGrath, M. A., Wong, M. C., and Cooper, J. F. (2007). The spatial morphology of Europa's near-surface O_2 atmosphere. *Icarus*, 191(2):755–764.

Chhabra, S., Gacesa, M., Khalil, M. S., Al Ghaferi, A., and El-Kork, N. (2023). A quantum-mechanical investigation of $O(^3P)$+ CO scattering cross sections at superthermal collision energies. *Monthly Notices of the Royal Astronomical Society*, 519(1):1253–1260.

Cosby, P. C. (1993). Electron-impact dissociation of oxygen. *The Journal of Chemical Physics*, 98(12):9560–9569.

Cunningham, N. J., Spencer, J. R., Feldman, P. D., Strobel, D. F., France, K., and Osterman, S. N. (2015). Detection of Callisto's oxygen atmosphere with the Hubble Space Telescope. *Icarus*, 254:178–189.

Dols, V. J., Bagenal, F., Cassidy, T. A., Crary, F. J., and Delamere, P. A. (2016). Europa's atmospheric neutral escape: Importance of symmetrical O_2 charge exchange. *Icarus*, 264:387–397.

Eviatar, A., Bar-nun, A., and Podolak, M. (1985). Europan surface phenomena. *Icarus*, 61(2):185–191.

Gacesa, M. and Kharchenko, V. (2014). Quantum reactive scattering of $O(^3P)$+H_2 at collision energies up to 4.4 eV. *The Journal of Chemical Physics*, 141(16).

Gacesa, M., Lillis, R. J., and Zahnle, K. J. (2020). $O(^3P)$+ CO_2 scattering cross-sections at superthermal collision energies for planetary aeronomy. *Monthly Notices of the Royal Astronomical Society*, 491(4):5650–5659.

Hall, D. T., Feldman, P. D., McGrath, M. A., and Strobel, D. F. (1998). The far-ultraviolet oxygen airglow of Europa and Ganymede. *The Astrophysical Journal*, 499(1):475.

Hall, D. T., Strobel, D. F., Feldman, P. D., McGrath, M. A., and Weaver, H. A. (1995). Detection of an oxygen atmosphere on Jupiter's moon Europa. *Nature*, 373(6516):677.

Hansen, C. J., Shemansky, D. E., and Hendrix, A. R. (2005). Cassini UVIS observations of Europa's oxygen atmosphere and torus. *Icarus*, 176(2):305–315.

Huebner, W. F. and Mukherjee, J. (2015). Photoionization and photodissociation rates in solar and blackbody radiation fields. *Planetary and Space Science*, 106:11–45.

Ip, W.-H., Williams, D. J., McEntire, R. W., and Mauk, B. H. (1998). Ion sputtering and surface erosion at Europa. *Geophysical research letters*, 25(6):829–832.

Johnson, R. E. (1990). *Energetic charged-particle interactions with atmospheres and surfaces*. Springer Science & Business Media.

Johnson, R. E., Killen, R. M., Waite Jr, J. H., and Lewis, W. S. (1998). Europa's surface composition and sputter-produced ionosphere. *Geophysical research letters*, 25(17):3257–3260.

Johnson, R. E., Lanzerotti, L. J., and Brown, W. L. (1982). Planetary applications of ion induced erosion of condensed-gas frosts. *Nuclear Instruments and Methods in Physics Research*, 198(1):147–157.

Johnson, R. E., Boring, J. W., Reimann, C. T., Barton, L. A., Sieveka, E. M., Garrett, J. W., Farmer, K. R., Brown, W. L., and Lanzerotti, L. J. (1983). Plasma ion-induced molecular ejection on the Galilean satellites: Energies of ejected molecules. *Geophysical research letters*, 10(9):892–895.

Kimmel, G. A. and Orlando, T. M. (1995). Low-energy (5–120 eV) electron-stimulated dissociation of amorphous D_2O ice: $D(^2S)$, $O(^3P_{2,1,0})$, and $O(^1D_2)$ yields and velocity distributions. *Physical review letters*, 75(13):2606.

Kliore, A. J., Hinson, D. P., Flasar, F. M., Nagy, A. F., and Cravens, T. E. (1997). The ionosphere of Europa from Galileo radio occultations. *Science*, 277(5324):355–358.

Kumar, S., Kumar, S., Gacesa, M., El-Kork, N., and Yamijala, S. S. R. K. C. (2023). Quantum scattering cross-sections for $O(^3P)+ N_2$ collisions for planetary aeronomy. *Monthly Notices of the Royal Astronomical Society*, 526(4):5675–5681.

Leblanc, F., Oza, A. V., Leclercq, L., Schmidt, C., Cassidy, T., Modolo, R., Chaufray, J.-Y., and Johnson, R. E. (2017). On the orbital variability of Ganymede's atmosphere. *Icarus*, 293:185–198.

Leblanc, F., Roth, L., Chaufray, J.-Y., Modolo, R., Galand, M., Ivchenko, N., Carnielli, G., Baskevitch, C., Oza, A., and Werner, A. (2023). Ganymede's atmosphere as constrained by HST/STIS observations. *Icarus*, 399:115557.

Lewkow, N. R. and Kharchenko, V. (2014). Precipitation of energetic neutral atoms and induced non-thermal escape fluxes from the Martian atmosphere. *The Astrophysical Journal*, 790(2):98.

Lucchetti, A., Plainaki, C., Cremonese, G., Milillo, A., Cassidy, T. A., Jia, X., and Shematovich, V. (2016). Loss rates of Europa's tenuous atmosphere. *Planetary and Space Science*, 130:14–23.

Marconi, M. L. (2007). A kinetic model of Ganymede's atmosphere. *Icarus*, 190:155–174.

McGrath, M. A., Lellouch, E., Strobel, D. F., Feldman, P. D., and Johnson, R. E. (2004). Satellite atmospheres. *Jupiter: The Planet, Satellites and Magnetosphere*, pages 457–483.

Miura, N., Hashimoto, K., Takahashi, K., Taniguchi, N., and Matsumi, Y. (2002). Electronic quenching of $O(^1D)$ by collisions with O_2: A theoretical study in a collinear case. *The Journal of chemical physics*, 116(13):5551–5556.

Oza, A. V., Leblanc, F., Johnson, R. E., Schmidt, C., Leclercq, L., Cassidy, T. A., and Chaufray, J.-Y. (2019). Dusk over dawn O_2 asymmetry in Europa's near-surface atmosphere. *Planetary and Space Science*, 167:23–32.

Pan, T.-J., Wilson, T. J., and Stephani, K. A. (2019). Vibrational state-specific model for dissociation and recombination of the $O_2(^3\Sigma_g^-)+O(^3P)$ system in DSMC. *The Journal of chemical physics*, 150(7).

Plainaki, C., Cassidy, T. A., Shematovich, V. I., Milillo, A., Wurz, P., Vorburger, A., Roth, L., Galli, A., Rubin, M., Blöcker, A., Brandt, P. C., Crary, F., Dandouras, I., Jia, X., Grassi, D., Hartogh, P., Lucchetti, A., McGrath, M., Mangano, V., Mura, A., Orsini, S., Paranicas, C., Radioti, A., Retherford, K. D., Saur, J., and Teolis, B. (2018). Towards a global unified model of Europa's tenuous atmosphere. *Space Science Reviews*, 214(1):1–71.

Plainaki, C., Milillo, A., Mura, A., Orsini, S., and Cassidy, T. (2010). Neutral particle release from Europa's surface. *Icarus*, 210(1):385–395.

Plainaki, C., Milillo, A., Mura, A., Orsini, S., Massetti, S., and Cassidy, T. (2012). The role of sputtering and radiolysis in the generation of Europa exosphere. *Icarus*, 218(2):956–966.

Plainaki, C., Milillo, A., Mura, A., Saur, J., Orsini, S., and Massetti, S. (2013). Exospheric O_2 densities at Europa during different orbital phases. *Planetary and Space Science*, 88:42–52.

Roth, L. (2021). A stable H_2O atmosphere on Europa's trailing hemisphere from HST Images. *Geophysical Research Letters*, 48(20):e2021GL094289.

Roth, L., Alday, J., Becker, T. M., Ivchenko, N., and Retherford, K. D. (2017a). Detection of a hydrogen corona at Callisto. *Journal of Geophysical Research: Planets*, 122(5):1046–1055.

Roth, L., Ivchenko, N., Gladstone, G. R., Saur, J., Grodent, D., Bonfond, B., Molyneux, P. M., and Retherford, K. D. (2021). A sublimated water atmosphere on Ganymede detected from Hubble Space Telescope observations. *Nature Astronomy*, 5(10):1043–1051.

Roth, L., Retherford, K. D., Ivchenko, N., Schlatter, N., Strobel, D. F., Becker, T. M., and Grava, C. (2017b). Detection of a hydrogen corona in HST Lyα images of Europa in transit of Jupiter. *The Astronomical Journal*, 153(2):67.

Roth, L., Saur, J., Retherford, K. D., Strobel, D. F., Feldman, P. D., McGrath, M. A., Spencer, J. R., Blöcker, A., and Ivchenko, N. (2016). Europa's far ultraviolet oxygen aurora from a comprehensive set of HST observations. *Journal of Geophysical Research: Space Physics*, 121(3):2143–2170.

Saur, J., Feldman, P. D., Roth, L., Nimmo, F., Strobel, D. F., Retherford, K. D., McGrath, M. A., Schilling, N., Gerard, J.-C., and Grodent, D. (2011). Hubble space telescope/advanced camera for surveys observations of Europa's atmospheric ultraviolet emission at eastern elongation. *The Astrophysical Journal*, 738(2):153.

Saur, J., Strobel, D. F., and Neubauer, F. M. (1998). Interaction of the Jovian magnetosphere with Europa: Constraints on the neutral atmosphere. *Journal of Geophysical Research: Planets*, 103(E9):19947–19962.

Schafer, D., Newman, J., Smith, K., and Stebbings, R. (1987). Differential cross sections for scattering of 0.5-, 1.5-, and 5.0-keV oxygen atoms by He, N_2, and O_2. *Journal of Geophysical Research: Space Physics*, 92(A6):6107–6113.

Shematovich, V. I. (2006). Stochastic models of hot planetary and satellite coronas: Atomic oxygen in Europa's corona. *Solar System Research*, 40:175–190.

Shematovich, V. I. and Johnson, R. E. (2001). Near-surface oxygen atmosphere at Europa. *Advances in Space Research*, 27(11):1881–1888.

Shematovich, V. I., Johnson, R. E., Cooper, J. F., and Wong, M. C. (2005). Surface-bounded atmosphere of Europa. *Icarus*, 173(2):480–498.

Smith, G. R., Shemansky, D. E., Broadfoot, A. L., and Wallace, L. (1978). Monte Carlo modeling of exospheric bodies: Mercury. *Journal of Geophysical Research: Space Physics*, 83(A8):3783–3790.

Smith, H. T., Mitchell, D. G., Johnson, R. E., Mauk, B. H., and Smith, J. E. (2019). Europa neutral torus confirmation and characterization based on observations and modeling. *The Astrophysical Journal*, 871(1):69.

Smyth, W. H. and Marconi, M. L. (2006). Europa's atmosphere, gas tori, and magnetospheric implications. *Icarus*, 181(2):510–526.

Spencer, J. R., Tamppari, L. K., Martin, T. Z., and Travis, L. D. (1999). Temperatures on Europa from Galileo photopolarimeter-radiometer: Nighttime thermal anomalies. *Science*, 284(5419):1514–1516.

Szalay, J. R., Allegrini, F., Ebert, R. W., Bagenal, F., Bolton, S. J., Fatemi, S., McComas, D. J., Pontoni, A., Saur, J., Smith, H. T., Strobel, D. F., Vance, S. D., Vorburger, A., and Wilson, R. J. (2024). Oxygen production from dissociation of Europa's water-ice surface. *Nature Astronomy*.

Szalay, J. R., Smith, H. T., Zirnstein, E. J., McComas, D. J., Begley, L. J., Bagenal, F., Delamere, P. A., Wilson, R. J., Valek, P. W., Poppe, A. R., Nénon, Q., Allegrini, F., Ebert, R. W., and Bolton, S. J. (2022). Water-group pickup ions from Europa-genic neutrals orbiting Jupiter. *Geophysical Research Letters*, page e2022GL098111.

Teolis, B. D., Wyrick, D. Y., Bouquet, A., Magee, B. A., and Waite, J. H. (2017). Plume and surface feature structure and compositional effects on Europa's global exosphere: Preliminary Europa mission predictions. *Icarus*, 284:18–29.

Turc, L., Leclercq, L., Leblanc, F., Modolo, R., and Chaufray, J.-Y. (2014). Modelling Ganymede's neutral environment: a 3D test-particle simulation. *Icarus*, 229:157–169.

Vorburger, A., Fatemi, S., Galli, A., Liuzzo, L., Poppe, A. R., and Wurz, P. (2022). 3D Monte-Carlo simulation of Ganymede's water exosphere. *Icarus*, 375:114810.

Vorburger, A., Fatemi, S., Mogan, S. R. C., Galli, A., Liuzzo, L., Poppe, A. R., Roth, L., and Wurz, P. (2024). 3D Monte-Carlo simulation of Ganymede's atmosphere. *Icarus*, 409:115847.

Vorburger, A. and Wurz, P. (2018). Europa's ice-related atmosphere: the sputter contribution. *Icarus*, 311:135–145.

Waite Jr, J. H., Greathouse, T. K., Carberry Mogan, S. R., Sulaiman, A. H., Valek, P., Allegrini, F., Ebert, R. W., Gladstone, G. R., Kurth, W. S., Connerney, J. E. P., Clark, G., Bagenal, F., Duling, S., Romanelli, N., Bolton, S., Vorburger, A., Paranicas, C., Kollmann, P., Mauk, B., Hansen, C., Buccino, D., Johnson, R. E., Wilson, R. J., and

Teolis, B. (2024). Magnetospheric-ionospheric-atmospheric implications from the Juno flyby of Ganymede. *Journal of Geophysical Research: Planets*, 129(4):e2023JE007859.